

# A flash in the dark: UVES/VLT high resolution spectroscopy of GRB afterglows<sup>1</sup>

F. Fiore<sup>1</sup>, V. D’Elia<sup>1</sup>, D. Lazzati<sup>2,3</sup>, R. Perna<sup>3,4</sup>, L. Sbordone<sup>1,5</sup>, G. Stratta<sup>1,6</sup>, E.J.A. Meurs<sup>7</sup>, P. Ward<sup>7</sup>, L.A. Antonelli<sup>1</sup>, G. Chincarini<sup>8</sup>, S. Covino<sup>9</sup>, A. Di Paola<sup>1</sup>, A. Fontana<sup>1</sup>, G. Ghisellini<sup>9</sup>, G. Israel<sup>1</sup>, F. Frontera<sup>10</sup>, G. Marconi<sup>1,5</sup>, L. Stella<sup>1</sup>, M. Vietri<sup>11</sup>, F. Zerbi<sup>9</sup>

<sup>1</sup>INAF–Osservatorio Astronomico di Roma, Via Frascati 33, I–00044 Monteporzio Catone, Italy;

<sup>2</sup> Institute of Astronomy, University of Cambridge, Madingley Road, Cambridge, UK;

<sup>3</sup> Department of Astrophysical and Planetary Science, CU Boulder, Boulder, 80309, USA;

<sup>4</sup> Princeton University Observatory, Princeton, NJ 08544–1001, USA;

<sup>5</sup> European Southern Observatory, Casilla 19001, Santiago, Chile;

<sup>6</sup> Dipartimento di Fisica, Università’ di Roma La Sapienza, Italy;

<sup>7</sup> Dunsink Observatory, Castleknock, Dublin 15, Ireland;

<sup>8</sup> Università’ di Milano Bicocca, Piazza della Scienza 3, 20126 Milano, Italy

<sup>9</sup> INAF, Osservatorio Astronomico di Brera, via E. Bianchi 46, 23807 Merate (LC), Italy.

<sup>10</sup> Dipartimento di Fisica, Università’ di Ferrara, via Paradiso 12, 44100 Ferrara, Italy;

<sup>11</sup> Scuola Normale Superiore, I–56100 Pisa, Italy.

(version: 2 February 2005)

## ABSTRACT

We present the first high resolution ( $R=20000\text{--}45000$ , corresponding to 14 km/s at 4200Å to 6.6 km/s at 9000Å ) observations of the optical afterglow of Gamma Ray Bursts. GRB 020813 and GRB 021004 were observed by UVES@VLT 22.19 hours and 13.52 hours after the trigger, respectively. These spectra show that the inter–stellar matter of the GRB host galaxies is complex, with many components contributing to each main absorption system, and spanning a total velocity range of up to about 3000 km/s. Several narrow components are resolved down to a width of a few tens of km/s. In the case of GRB 021004 we detected both low and high ionization lines. Combined with photoionization results obtained with CLOUDY, the ionization parameters of the various systems are consistent with a remarkably narrow range with no clear trend with system velocity. This can be interpreted as due to density fluctuations on top of a regular  $R^{-2}$  wind density profile.

---

<sup>1</sup>Based on observations collected at the European Southern Observatory, ESO, the VLT/Kueyen telescope, Paranal, Chile, in the framework of programs 69.A–0516(B) and 70.A–0599(B)

*Subject headings:* gamma rays: bursts – cosmology: observations – galaxies: abundances – ISM

## 1. Introduction

For a few hours after their onset, Gamma Ray Bursts (GRBs) are the brightest beacons in the far Universe, offering a superb opportunity to investigate both GRB physics and high redshift galaxies. Tens of minutes after a GRB, its optical afterglow can be as bright as magnitude 13–15; a few hours later a magnitude of 16–19 is often achieved. Bright examples are the cases of GRB 990123 ( $z=1.600$ ), for which the reverse shock reached  $R=9$ –10 mag 1 minute after the GRB and the optical afterglow reached  $R=14$  mag 12 minutes after the GRB (e.g. Akerlof et al. 1999, Galama et al. 1999), and GRB 030329 ( $z=0.1685$ ), for which the optical afterglow reached  $R=12.7$  mag at 1.5 hours from the GRB and decreased down to  $R=19$  mag after  $\sim 10$  days (e.g. Price et al. 2003; Stanek et al. 2003). High resolution (a few tens of km/s in the optical band), high quality (signal to noise  $> 10$  per resolution element) spectra can therefore be gathered, provided that the afterglow is observed rapidly by 8m class telescopes. Since GRBs are associated with the collapse of massive stars (see Woosley 1993, Paczynski 1998, MacFadyen & Woosley 1999, Vietri & Stella 1998 for theoretical reasons and Galama et al. 1998, Stanek et al. 2003, Hjorth et al. 2003 and Della Valle et al. 2003 for observational reasons), this is expected to open a new window in the study of the environment in which intermediate to high redshift star-formation occurs and, in particular, on the physical, chemical and dynamical state of the inter-stellar matter (ISM) of the GRB host galaxies.

The study of  $z \gtrsim 1$  galaxies has so far mostly relied upon Lyman-break galaxies (LBGs) at  $z = 3 - 4$  (see e.g. Steidel et al. 1999) and galaxies which happen to be along the line of sight to bright background QSOs. Some of these systems are associated with Damped Ly $\alpha$  systems (DLA, see e.g. Pettini et al. 1997). However, LBGs are characterized by pronounced star-formation and their inferred chemical abundances may be related to these regions rather than being representative of typical high  $z$  galaxies. Metal line systems associated to DLAs along the line of sight to quasars probe mainly galaxy haloes, rather than their bulges or discs. Furthermore, it is not clear whether galaxies associated with DLAs are truly representative of the whole high- $z$  galaxy population. GRB afterglows provide an independent tool to study the ISM of high  $z$  galaxies. Savaglio, Fall & Fiore (2003) studied the metal abundances in three GRB host galaxies using low-medium resolution spectroscopy and a curve of growth analysis. They found metal column densities

higher than in QSO-DLAs and a strong inverse correlation between  $[\text{Si}/\text{Zn}]$ ,  $[\text{Cr}/\text{Zn}]$  and  $[\text{Fe}/\text{Zn}]$  and the Zn column density, indicating a dense environment and large dust depletion. On the other hand, Vreeswijk et al. (2004) found indications for a relatively low metallicity and low dust content in the ISM of the  $z=3.372$  host galaxy of GRB 030323, using FORS2 low and intermediate resolution spectroscopy. Using again a curve of growth analysis, and taking advantage of ultra-deep *Gemini* multi-object spectrograph observations, Savaglio et al. (2004) studied the ISM of a sample of faint K band selected galaxies at  $1.4 < z < 2.0$ , finding Mg II and Fe II abundances much higher than in QSO-DLAs and similar to those in GRB host galaxies. A much better job can be done with high resolution ( $R > 20000$ ) observations because: (i) lines can be separated; (ii) metal column densities can be measured through a fit to the line profile; (iii) fainter lines can be measured; (iv) information on the gas dynamics in the GRB host galaxies can be derived. Furthermore, as suggested by the comparison of the Vreeswijk et al. (2004) and the Savaglio et al. (2004) studies, GRB afterglows allow us to probe galaxy ISM at much higher redshifts than even ultra-deep, standard galaxy spectroscopy, such as the Gemini Deep Deep Survey.

For all these reasons we started a pilot program to observe bright GRB afterglows of promptly localized GRBs with UVES@VLT. The program has been conceived and designed to make full use of the GRB afterglows discovered by the GRB-dedicated *Swift* mission, launched on November 20 2004<sup>2</sup>. *Swift* will provide GRB positions ( $< 4'$  precision) in  $< 10$  s, X-ray afterglow positions ( $3''$  precision) in  $< 100$  s, and an optical finding chart in  $< 300$  s, with a few arcsec to sub-arcsec position accuracy, thus revolutionizing fast response multiwavelength studies of GRBs.

This article concentrates on high resolution spectroscopy of two GRB afterglows. The HETE-2 FREGATE, WXM and SXC instruments detected GRB 021004 on 2002 Oct. 4 12:06:13.57 UT (Shirasaki et al. 2002) and GRB 020813 on 2002 Aug. 13 02:44:19.17 UT (Villasenor et al. 2002). The WXM flight localization software produced a reliable and relatively accurate position 49 seconds after the burst for GRB 021004 (error box of  $30'$  radius) and 4 minutes after the burst for GRB 020813 (error box of  $14'$  radius). Bright optical counterparts were identified 10 minutes and 1.9 hours after the triggers by Fox et al. (2002, 2003), and Fox, Blake & Price (2002) respectively. Ground analysis of the HETE2 data performed a few hours after each GRB improved the localization of the event, providing error boxes of  $2'$  and  $1'$  radius, respectively. UVES observations started 13.52 hours after the GRB 021004 trigger, (Savaglio et al. 2002) and 22.19 hours after the GRB 020813 trigger (Fiore et al. 2002).

---

<sup>2</sup><http://swift.gsfc.nasa.gov>

Optical low to intermediate resolution spectroscopy of the afterglow of GRB 021004 was obtained by Moller et al. (2003), Mirabal et al. (2003), Matheson et al. (2003), Schaefer et al. (2003). One of the main conclusion of these works is that density fluctuations on top of a regular wind density profile are able to explain both the presence of strong, blue-shifted, high ionization absorption line systems and irregularities in the optical light curve. Schaefer et al. (2003) propose a scenario where a clumpy wind originates from a massive star progenitor (a Wolf-Rayet star), while Mirabal et al. (2003) suggest that the ionized absorption takes place in a fragmented shell nebula around the GRB progenitor. Optical spectropolarimetry of the afterglow of GRB 020813 has been presented by Barth et al. (2003) who report the detection of strong absorption systems at  $z=1.223$  and  $z=1.255$ . A further analysis of the Keck LRIS spectrum is presented by Savaglio et al. (2004). The present paper reports the results of higher resolution spectroscopy of both afterglows.

Both GRBs were observed in the X-rays too by the Chandra High Energy Transmission Grating System, which has a resolution of  $\sim 1000$  at 1 keV (Butler et al. 2003 and references therein). Both observations lasted about 80 ks and started 21 hours and 20 hours after the GRB event for GRB 020813 and GRB 021004 respectively. Fading X-ray afterglows were detected in both cases with decay indices of  $-1.38 \pm 0.06$  and  $-0.9 \pm 0.1$ , consistent with the values reported for the optical afterglows by Covino et al. (2003) and Holland et al. (2003). The time averaged fluxes were  $2.2 \times 10^{-12}$  erg cm $^{-2}$  s $^{-1}$  and  $6.3 \times 10^{-13}$  erg cm $^{-2}$  s $^{-1}$  respectively. The X-ray spectra are consistent with power laws of energy index of  $-0.85 \pm 0.04$  and  $-1.01 \pm 0.08$  reduced at low energy by Galactic column density (which is rather high in the direction of GRB 020813,  $N_{HGal} = 7.5 \times 10^{20}$  cm $^{-2}$ , and is  $N_{HGal} = 4.2 \times 10^{20}$  cm $^{-2}$  in the direction of GRB 021004). The upper limits to the rest frame X-ray absorbing column are of the order of a few  $\times 10^{20}$  in both cases. Butler et al. (2003) report the detection of an emission line at 1.3 keV at the  $3.3\sigma$  confidence level, interpreted as a SXVI  $\alpha$  line blue-shifted by 0.12c.

## 2. Observations and data reduction

In the framework of ESO programs 69.A-0516 and 70.A-0599 we observed the afterglows of GRB 020813 and GRB 021004 with the high resolution UV-visual echelle spectrograph (UVES, Dekker et al. 2000), mounted at the VLT-UT2 telescope. Table 1 gives the log of the observations used in this paper. A further 1 hour dichroic 1 observation is available in the ESO archive, but we were not able to extract a reliable spectrum from this observation, which has therefore been discarded. In order to maximize the signal to noise ratio the CCD was rebinned  $2 \times 2$  pixels. The data reduction has been performed

using the UVES pipeline<sup>3</sup>. The final useful spectra extend from about 4250Å to about 9400Å and were rebinned to 0.1Å to increase the signal to noise. The resulting resolution element, set to two pixels, ranges then from 14 km/s at 4200Å to 6.6 km/s at 9000Å . The noise spectrum, used to determine the errors on the best fit line parameters, has been calculated from the real background subtracted and rebinned spectrum using line free regions. This therefore takes into account both statistical errors and systematic errors in the pipeline processing and background subtraction. Table 2 gives the signal to noise ratio per 0.1Å pixel at different wavelengths for the 4 spectra in Table 1. Figure 1 plots the full UVES spectrum of GRB 021004, for which both UVES dichroics, and both red and blue arms, were used, allowing us to obtain a particularly wide spectral coverage, extending from ~4250Å to ~9400Å . A further dichroic 1, blue arm image, covering the band 3400Å – 3900 Å was obtained, but the signal to noise is too low to allow a reliable extraction of the spectrum in this band. Figure 2 plots the full UVES spectrum of GRB 020813. This spectrum, as well as the spectrum in figure 1, was smoothed with a gaussian function with  $\sigma = 1.5$  pixels. Tables 3 and 4 give the equivalent width of all lines detected in the UVES spectra for the two GRB afterglows, along with their identification. The equivalent widths are computed at the redshift of the absorption systems. For the GRB host galaxy identified systems and the 2 main intervening systems at  $z=1.60$  and  $1.38$  we report also faint lines with (signal to noise  $> 1$ ). Unidentified lines are reported only if the signal to noise is  $> 3$ . Their equivalent widths are computed at zero redshift.

### 3. Column densities

In this paper we focus on the systems which are likely to be associated with the GRB host galaxies. The line fitting was performed using the MIDAS package FITLYMAN (Fontana & Ballester 1995). This uses a Voigt profile and yields independently the column density  $N$  and the Doppler parameter  $b$  for each absorption component. For each

---

<sup>3</sup><http://www.eso.org/observing/dfo/quality/UVES/pipeline/>

**Table 1: Journal of observations**

Date UT	Dichroic	B. Arm C.W.	R. Arm C.W.	slit <sup>a</sup>	seeing <sup>a</sup>	exposure <sup>b</sup>	time since GRB <sup>c</sup>
14/08/02 00:55:25	1	3460Å	5800Å	1	$\lesssim 1$	60	22.19
05/10/02 01:37:37	2	4370Å	8600Å	1	$\lesssim 1$	30	13.52
05/10/02 02:10:53	1	3460Å	5800Å	1	$\lesssim 1$	30	14.08
05/10/02 04:09:54	1	3460Å	5800Å	1	$\lesssim 1$	60	16.06

<sup>a</sup>arcsec; <sup>b</sup>min; <sup>c</sup>hr

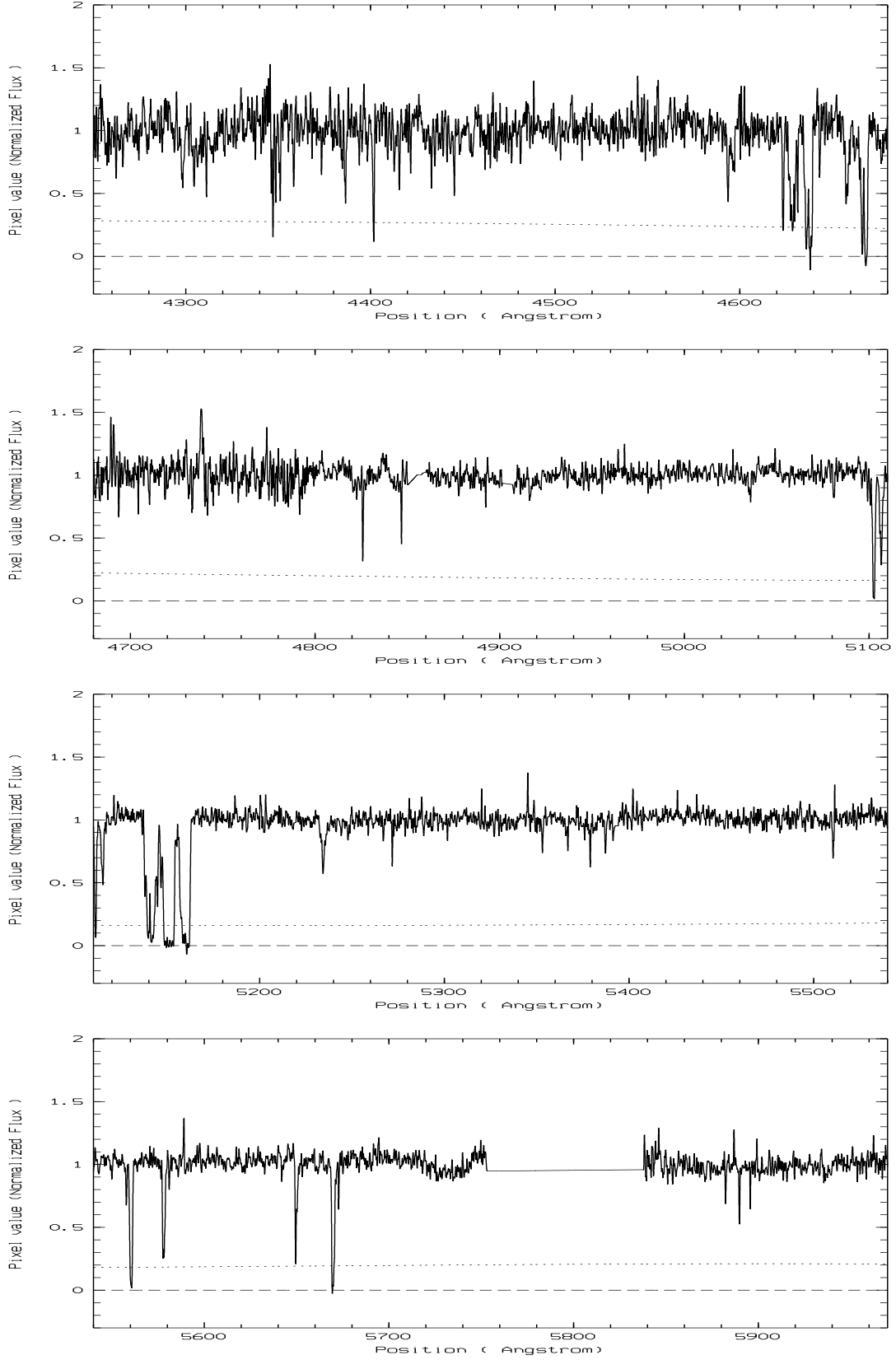


Fig. 1.— UVES spectrum of the GRB 021004 afterglow smoothed with a gaussian function with  $\sigma = 1.5$  pixel . The dotted line is the error spectrum

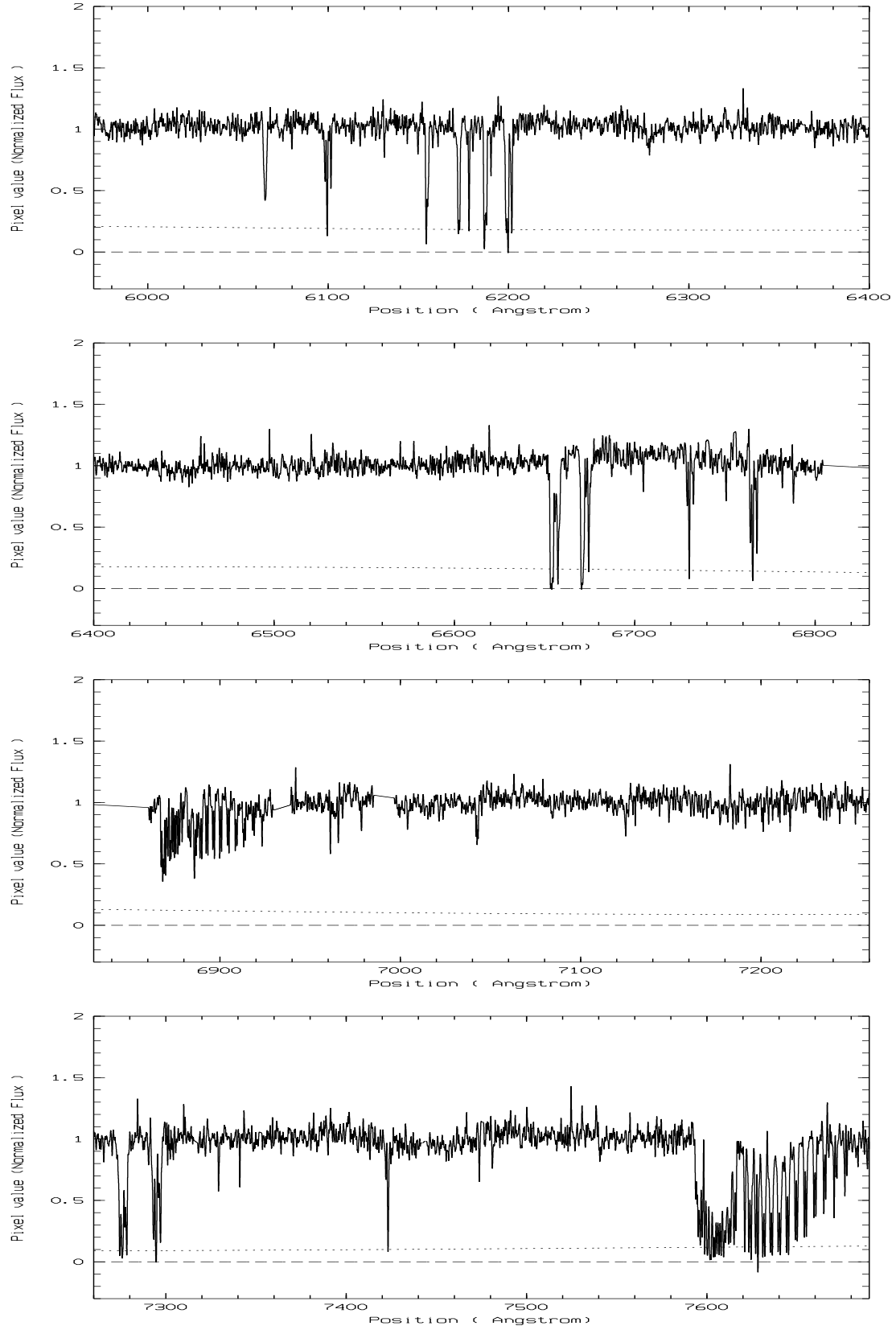


Fig. 1.— continued

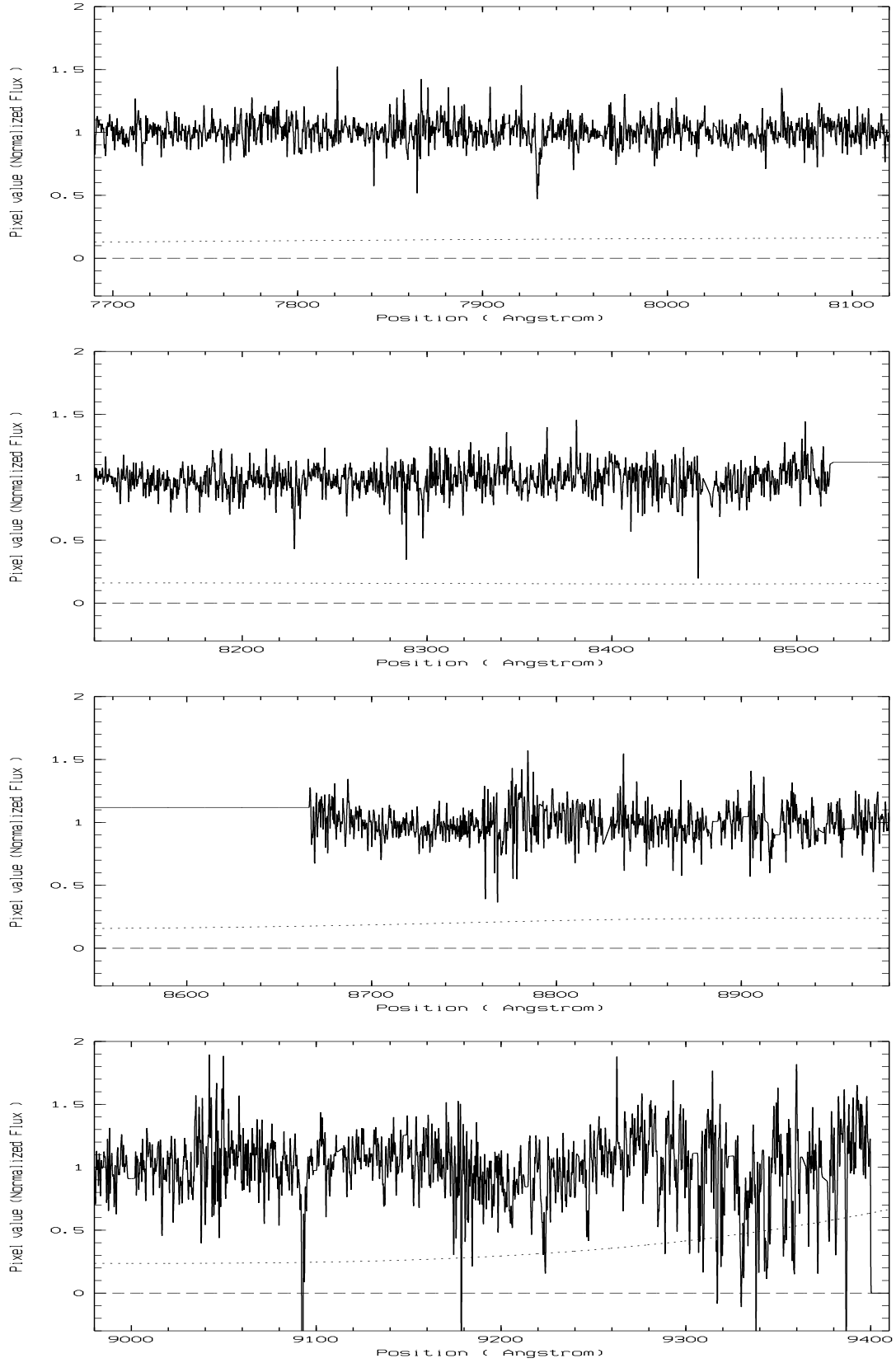


Fig. 1.— continued



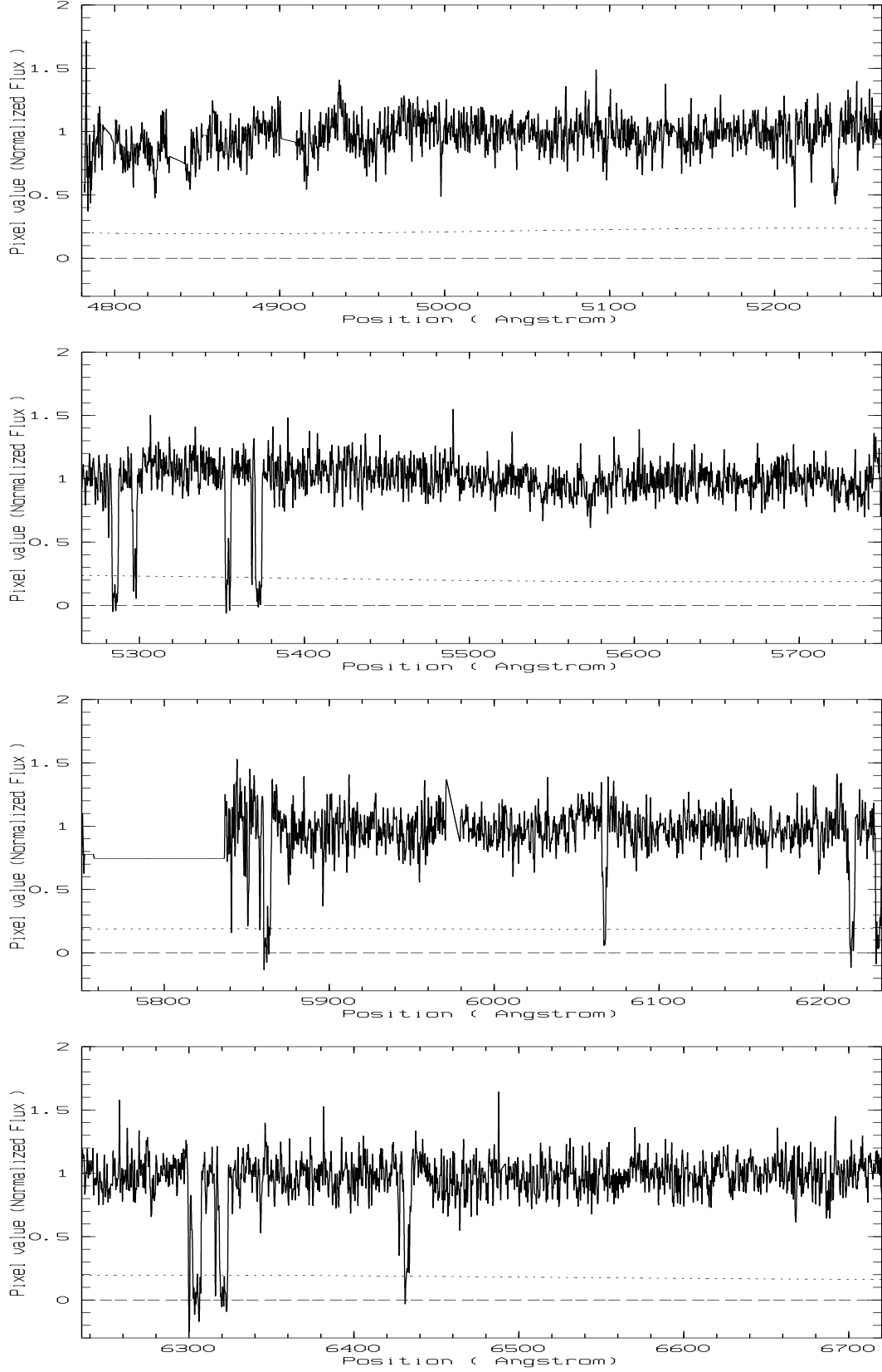


Fig. 2.— UVES spectrum of the GRB 020813 afterglow smoothed with a gaussian function with  $\sigma = 1.5$  pixel . The dotted line is the error spectrum

absorption system several lines, spread over the entire spectral range covered by the UVES observations, were fitted simultaneously, using the same number of components for each line, and the same redshift and  $b$  value for each component.

### 3.1. GRB 021004

For this GRB we consider the absorption systems at the following redshifts and velocities (in km/s) with respect to the Ly $\alpha$  emission of the host galaxy (Mirabal et al. 2003):  $z=2.328$ ,  $v=0$  (system A in figure 3);  $z=2.328$ ,  $v=-139$  km/s (system B);  $z=2.328$ ,  $v=-224$  km/s (system C);  $z=2.321$ ;  $z=2.298$ ;  $z=2.296$ . For these systems we detected C IV, C II, Si IV, Al II, Al III, Mg II and Fe II lines (see Table 3). We report in the table also the tentative identification of a Si II $\lambda$ 1304 line at  $z=2.2953$ . This is close but not coincident with the redshift of systems  $z=2.296$ . We therefore consider this identification uncertain, and we do not consider this line in the following analysis.

Unfortunately, the Ly $\alpha$  absorption associated with the  $z=2.328$  systems falls exactly in the gap between the dichroic 1 and 2 blue arm spectra, and therefore is not covered in this study. Zn II and Cr II absorption lines for the main  $z=2.328$  and  $z=2.321$  systems fall in the region affected by atmospheric telluric features (see figure 1) and are therefore not accessible.

Figure 3 shows the C IV and Si IV doublets of the above 6 systems. Note that the C IV $\lambda$ 1548 lines of the  $z=2.328$  A,B,C systems are strongly blended with the C IV $\lambda$ 1550 line of the  $z=2.321$  system, while the Si IV $\lambda$ 1404 line of the  $z=2.298$  system is blended with the Si IV $\lambda$ 1393 line of the  $z=2.321$  system. Each of the six systems actually comprises several components, within a velocity range of several tens of km/s. For this reason the identification of the different systems is somewhat subjective, the true message being that the geometry and kinematics of the ISM clouds probed by the GRB line of sight are

Table 2: **Signal to noise ratio**

$\lambda$	14/08/02 00hr	05/10/02 01hr-02hr	05/10/02 04hr
4250Å		3.6	
5000Å	4.7	5.9	9.3
6000Å	5.6	5.4	11.2
7000Å	5.9	9.8	10.2
7800Å		6.8	
9250Å		2.9	

Table 3: **GRB 021004 UVES line identifications**

$\lambda(\text{\AA})$	$W_{rest}(\text{\AA})^a$	ID	z
4298.40	0.13±0.02	?Si II $\lambda$ 1304.37?	?2.2953?
4301.73	0.06±0.03	Si II $\lambda$ 1808.01	1.3793-8
4304.53	0.09±0.03	Si II $\lambda$ 1808.01	1.3807
4311.20	0.16±0.08		
4346.30	0.27±0.08	Al II $\lambda$ 1670.79	1.6014
4347.25	0.18±0.03	Al II $\lambda$ 1670.79	1.6019
4348.60	0.11±0.03	Al II $\lambda$ 1670.79	1.6028
4350.95	0.53±0.08		
4358.28	0.35±0.08		
4398.34	0.06±0.03	C II $\lambda$ 1334.53	2.2958
4401.68	0.24±0.02	C II $\lambda$ 1334.53	2.2981-4 +
		?C II* $\lambda$ 1335.70?	?2.2958?
4415.50	0.10±0.03	Al III $\lambda$ 1854.71	1.3807
4441.34	0.04±0.02	C II $\lambda$ 1334.53	2.328
4445.35	0.09±0.02	C II* $\lambda$ 1335.70	2.328
4593.59	0.15±0.02	Si IV $\lambda$ 1393.76	2.2958
4596.71	0.02±0.02	Si IV $\lambda$ 1393.76	2.2981-4
4623.48	0.21±0.02	Si IV $\lambda$ 1402.77	2.2958
4626.41	0.02±0.02	Si IV $\lambda$ 1402.77	2.2981-4
4629.72	0.40±0.02	Si IV $\lambda$ 1393.76	2.321
4631.35	0.30±0.07		
4635.85	0.65±0.07		
4637.38	3.63±0.07		
4638.01	0.31±0.02	Si IV $\lambda$ 1393.76	2.328
4643.19	0.25±0.07		
4658.07	0.27±0.02	Si IV $\lambda$ 1402.77	2.321
4666.28	1.07±0.07		
4668.38	0.56±0.02	Si IV $\lambda$ 1393.76	2.328
5102.54	0.50±0.02	C IV $\lambda$ 1548.20	2.2958
5106.50	0.35±0.02	C IV $\lambda$ 1548.20	2.2981-4
5111.04	0.33±0.02	C IV $\lambda$ 1550.77	2.2958
5114.82	0.16±0.02	C IV $\lambda$ 1550.77	2.2981-4
5141.11	1.74±0.02	C IV $\lambda$ 1448.20	2.321
5150.4	2.10±0.02	C IV $\lambda$ 1550.77	2.321 +
		C IV $\lambda$ 1448.20	2.328
5159.66	1.57±0.02	C IV $\lambda$ 1550.77	2.328
5510.62	0.05±0.02	Al II $\lambda$ 1670.79	2.2981-4
5560.30	0.47±0.02	Al II $\lambda$ 1670.79	2.328
5577.71	1.47±0.03	Fe II $\lambda$ 2344.21	1.3793-8
5580.81	0.07±0.03	Fe II $\lambda$ 2344.21	1.3807
5592.94	0.14±0.06		
5649.59	0.31±0.03	Fe II $\lambda$ 2374.21	1.3793-8
5669.68	0.67±0.03	Fe II $\lambda$ 2382.77	1.3793-8
6064.56	0.60±0.06		
6098.32	0.22±0.06		

Errors are 67% confidence intervals. <sup>a</sup> the equivalent width of unidentified lines is computed at zero redshift; ? = uncertain identification. In many cases several components contribute to a single line in one entry of the table. In these cases either the redshift is given with only 4 digits or it is given as a range. A + sign indicates that a line is partly blended with the

Table 3: **GRB 021004 UVES line identifications, continued.**

$\lambda(\text{\AA})$	$W_{rest}(\text{\AA})^a$	ID	z
6099.33	0.19±0.02	Fe II $\lambda$ 2344.21	1.6019
6101.32	0.09±0.02	Fe II $\lambda$ 2344.21	1.6028
6154.64	0.52±0.03	Fe II $\lambda$ 2586.65	1.3793-8
6158.03	0.01±0.03	Fe II $\lambda$ 2586.65	1.3807
6160.76	0.17±0.06		
6172.42	0.35±0.02	Al III $\lambda$ 1854.72	2.328
6176.74	0.21±0.06		
6177.88	0.17±0.02	Fe II $\lambda$ 2374.46	1.6019
6180.04	0.14±0.05		
6186.51	0.25±0.02	Al III $\lambda$ 1862.79	2.321 +
6186.99	0.11±0.02	Fe II $\lambda$ 2600.17	1.3793-8
6187.81	0.05±0.02	Fe II $\lambda$ 2600.17	1.3798
6190.23	0.12±0.02	Fe II $\lambda$ 2600.17	1.3807
6199.36	0.11±0.02	Al III $\lambda$ 1862.79	2.328 +
6198.4			
6199.53	0.29±0.02	Fe II $\lambda$ 2382.77	1.6019
6201.66	0.28±0.02	Fe II $\lambda$ 2382.77	1.6028
6653.88	0.89±0.02	Mg II $\lambda$ 2796.35	1.3793-8
6655.88	0.24±0.02	Mg II $\lambda$ 2796.35	1.3802
6657.60	0.47±0.02	Mg II $\lambda$ 2796.35	1.3807
6671.00	0.78±0.02	Mg II $\lambda$ 2803.53	1.3793-8
6672.73	0.06±0.02	Mg II $\lambda$ 2803.53	1.3802
6674.77	0.32±0.02	Mg II $\lambda$ 2803.53	1.3807
6730.16	0.25±0.02	Fe II $\lambda$ 2586.65	1.6019
6732.55	0.09±0.02	Fe II $\lambda$ 2586.65	1.6028
6750.64	0.08±0.02	Mn II $\lambda$ 2594.50	1.6019
6764.18	0.43±0.04		
6765.43	0.25±0.02	Fe II $\lambda$ 2600.17	1.6019
6767.79	0.17±0.02	Fe II $\lambda$ 2600.17	1.6028
6768.78	0.18±0.04		
6781.81	0.04±0.02	Mn II $\lambda$ 2606.46	1.6019
6788.06	0.03±0.02	Mg I $\lambda$ 2852.94	1.3793-8
7003.91	0.12±0.03		
7041.91	0.12±0.03		
7042.52	0.11±0.03		
7043.25	0.10±0.03		
7274.52	0.26±0.01	Mg II $\lambda$ 2796.35	1.6014
7275.83	0.33±0.01	Mg II $\lambda$ 2796.35	1.6019
7277.28	0.49±0.01	Mg II $\lambda$ 2796.35	1.6024
7278.39	0.24±0.01	Mg II $\lambda$ 2796.35	1.6028
7293.12	0.27±0.01	Mg II $\lambda$ 2803.35	1.6014
7294.58	0.36±0.01	Mg II $\lambda$ 2803.53	1.6019
7295.91	0.04±0.01	Mg II $\lambda$ 2803.53	1.6024
7296.85	0.23±0.01	Mg II $\lambda$ 2803.53	1.6028
7422.05	0.04±0.01	Mg I $\lambda$ 2852.94	1.6014
7423.01	0.23±0.01	Mg I $\lambda$ 2852.94	1.6019

<sup>a</sup> the equivalent width of unidentified lines is computed at zero redshift. ? = uncertain identification. In many cases several components contribute to a single line in one entry of the table. In these cases either the redshift is given with only 4 digits or it is given as a

Table 3: **GRB 021004 UVES line identifications, continued.**

$\lambda(\text{\AA})$	$W_{rest}(\text{\AA})^a$	ID	z
7929.74	0.75 $\pm$ 0.05		
7929.53	0.08 $\pm$ 0.02	Fe II $\lambda$ 2382.77	2.328
7930.42	0.04 $\pm$ 0.02	Fe II $\lambda$ 2382.77	2.328
7931.03	0.03 $\pm$ 0.02	Fe II $\lambda$ 2382.77	2.328
8228.16	0.37 $\pm$ 0.05		
9178.45	0.75 $\pm$ 0.08		
9205.45	0.70 $\pm$ 0.09		
9216.41	0.04 $\pm$ 0.03	Mg II $\lambda$ 2796.35	2.2958
9222.70	0.09 $\pm$ 0.03	Mg II $\lambda$ 2796.35	2.2981
9223.62	0.18 $\pm$ 0.03	Mg II $\lambda$ 2796.35	2.2984
9246.33	0.09 $\pm$ 0.03	Mg II $\lambda$ 2803.53	2.2981
9247.39	0.12 $\pm$ 0.03	Mg II $\lambda$ 2803.53	2.2984
9330.33	0.57 $\pm$ 0.03	Mg II $\lambda$ 2803.53	2.328

<sup>a</sup> the equivalent width of unidentified lines is computed at zero redshift.

complex. Nevertheless, sticking to the above system identifications will be useful.

There are 13 lines in Table 3 associated with the z=2.328 systems, 5 lines associated with the z=2.321 system, and up to 17 lines associated to the z=2.296-2.298 systems. Some of these lines can be split further in several components. To test the robustness of the fit, in terms of accuracy and stability of the results, we performed many fits, using several combination of lines/systems. We found that the fits presented below are a good compromise between increasing the statistical precision of the fit, obtained increasing the number of lines fitted simultaneously, and the stability/repeatability of the results, which degraded increasing the number of fitted parameters, due to the increasingly complex shape of the  $\chi^2$  hyper-surface in the parameter space, that may contain many local minima.

For the z=2.328 A,B,C and z=2.321 systems we fitted simultaneously the C IV $\lambda\lambda$ 1550, 1548, C II $\lambda$ 1334, C II\* $\lambda$ 1335, Si IV $\lambda\lambda$ 1404, 1393 Al II  $\lambda$ 1670 and the Al III $\lambda$ 1854 line. We excluded from the fit the z=2.328 Al III $\lambda$ 1862 line because its blue wing is strongly blended with another line, and the z=2.321 Al III  $\lambda$ 1862 line because it is strongly blended with the Fe II $\lambda$ 2600 line of one of the components of the z=1.38 intervening system. For the same systems we also fitted the Fe II $\lambda$ 2382, Fe II $\lambda$ 2374 Fe II $\lambda$ 2344 Fe II $\lambda$ 1608, Mg II $\lambda$ 2803 and Mg II $\lambda$ 2796 lines simultaneously. Figure 4 shows the line spectra in velocity space, along with the best fit model, while Table 5 presents the best fit abundances along with the velocity shift of each system with respect to the redshift of the host galaxy, assumed to be 2.328 for GRB 021004 (Mirabal et al. 2003). We used 2 components for the z=2.328\_A system, and 1 component for the other 3 systems. The best fit doppler parameter b ranges from a minimum of 12 $\pm$ 6 km/s (one of the components of the z=2.328\_A system) up to

Table 4: **GRB 020813 UVES line identifications**

$\lambda(\text{\AA})$	$W_{rest}(\text{\AA})^a$	ID	z
4824.64	$1.06 \pm 0.05$		
4824.64	$0.59 \pm 0.05$		
4998.03	$0.47 \pm 0.05$		
5212.23	$0.18 \pm 0.03$	Fe II $\lambda$ 2344.21	1.2234
5236.74	$1.64 \pm 0.07$		
5281.33	$0.09 \pm 0.03$	Fe II $\lambda$ 2344.21	1.2529
5285.19	$1.70 \pm 0.03$	Fe II $\lambda$ 2344.21	1.255
5297.11	$0.85 \pm 0.03$	Fe II $\lambda$ 2382.77	1.2234
5353.61	$1.31 \pm 0.03$	Fe II $\lambda$ 2374.46	1.255
5368.21	$0.28 \pm 0.03$	Fe II $\lambda$ 2382.77	1.2529
5372.23	$1.63 \pm 0.03$	Fe II $\lambda$ 2382.77	1.255
5840.73	$0.44 \pm 0.06$		
5850.86	$0.73 \pm 0.06$		
5858.24	$0.23 \pm 0.02$	Fe II $\lambda$ 2600.17	1.2529
5862.33	$1.82 \pm 0.02$	Fe II $\lambda$ 2600.17	1.255
5896.25	$0.40 \pm 0.06$		
6067.05	$2.30 \pm 0.06$		
6216.93	$1.34 \pm 0.03$	Mg II $\lambda$ 2796.35	1.2234
6232.85	$1.36 \pm 0.03$	Mg II $\lambda$ 2803.53	1.2234
6300.13	$0.55 \pm 0.03$	Mg II $\lambda$ 2796.35	1.2529
6304.72	$2.38 \pm 0.03$	Mg II $\lambda$ 2796.35	1.255
6310.38	$0.30 \pm 0.06$		
6316.13	$0.30 \pm 0.03$	Mg II $\lambda$ 2803.53	1.2529
6321.11	$2.19 \pm 0.03$	Mg II $\lambda$ 2803.53	1.255
6343.49	$0.11 \pm 0.03$	Mg I $\lambda$ 2852.13	1.2234
6427.36	$0.24 \pm 0.03$	Mg I $\lambda$ 2852.13	1.2529
6432.12	$1.34 \pm 0.03$	Mg I $\lambda$ 2852.13	1.255
6686.87	$0.27 \pm 0.03$	Fe I $\lambda$ 2967.76	1.2529

Errors are 67% confidence intervals. <sup>a</sup> the equivalent width of unidentified lines is computed at zero redshift.

a maximum of  $107 \pm 10$  km/s (system  $z=2.321$ ). Of course different  $b$  values are obtained using an higher (or lower) number of components. Unfortunately the signal to noise ratio of our spectrum is not good enough to unambiguously identify the different components. On the other hand, we verified that the total best fit column density of each system is stable, within the statistical errors, changing the number of components in each system.

Similar series of fits were performed for the  $z=2.296$  and  $z=2.298$  systems, for which we used 1 and 2 components, respectively (see figure 5). Table 5 gives again the best fit abundances for these 2 systems. The best fit doppler parameter  $b$  ranges from  $9 \pm 7$  km/s to  $40 \pm 13$  km/s.

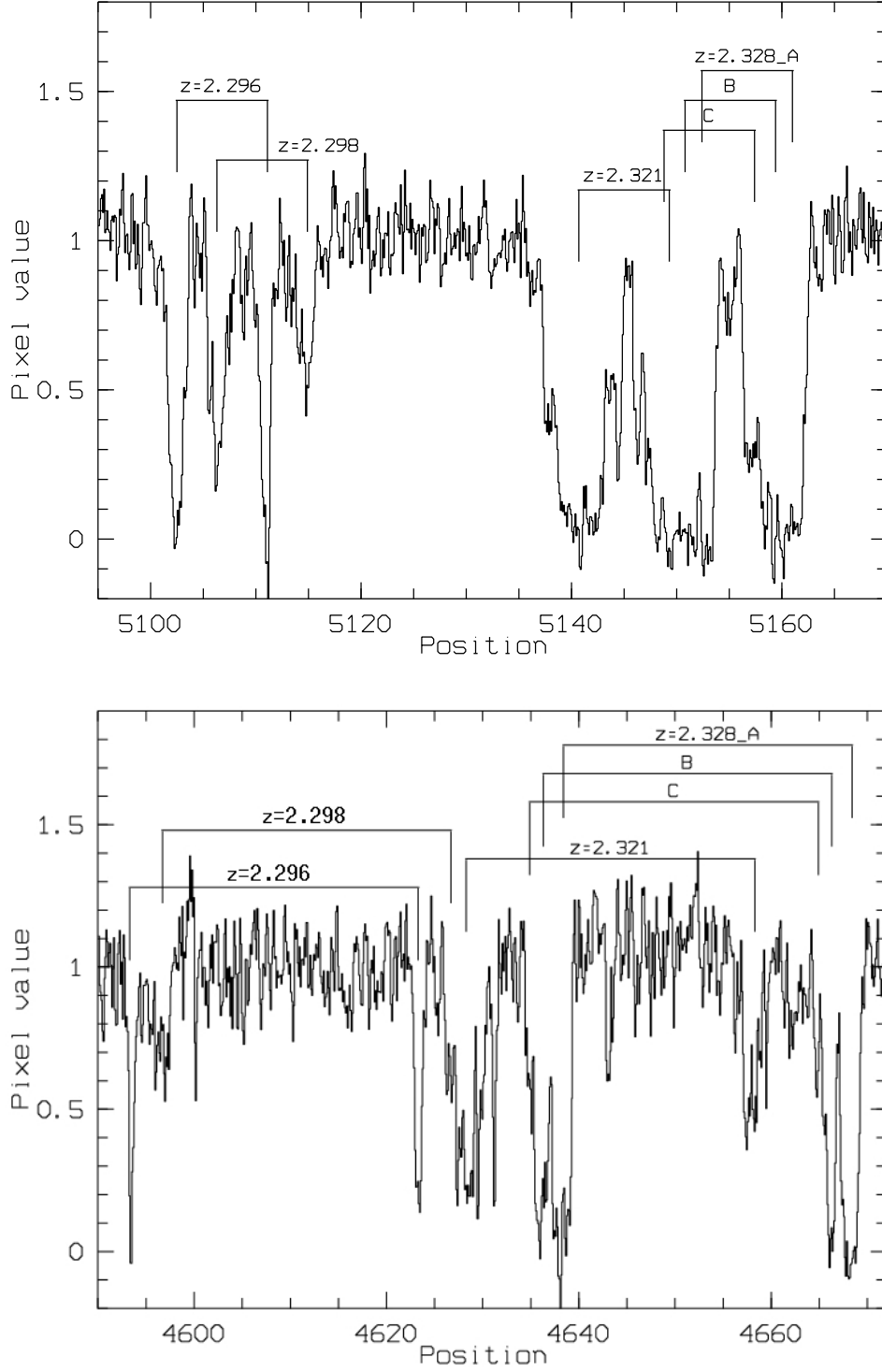


Fig. 3.— C IV (upper panel) and Si IV (lower panel) absorption systems in the UVES spectra of GRB 021004 for  $z=2.328$  (see Table 5).

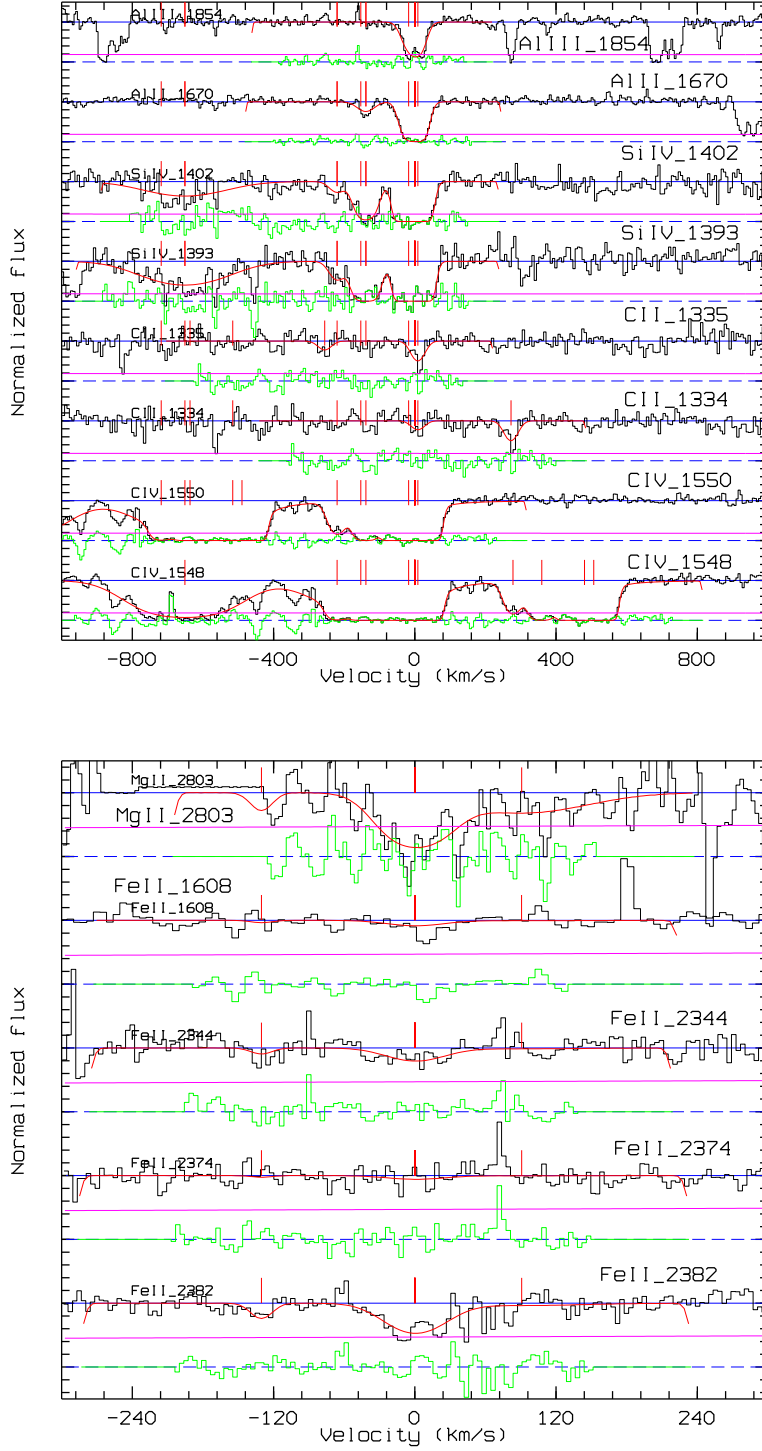


Fig. 4.— GRB 021004. Upper panel: UVES spectrum near the C IV  $\lambda\lambda$ 1550, 1548, C II  $\lambda$ 1334, C II  $\lambda$ 1335, Si IV  $\lambda\lambda$ 1404, 1393, Al II  $\lambda$ 1670 and Al III  $\lambda$ 1854 lines for the  $z=2.328$  and  $z=2.321$  systems in velocity space, along with the best fit model (solid line) and residuals (grey). Lower panel: same for the Fe II  $\lambda$ 2382, Fe II  $\lambda$ 2374, Fe II  $\lambda$ 2344, Fe II  $\lambda$ 1608 and Mg II  $\lambda$ 2803 lines. The zero in the velocity scale refers to the redshift of the host galaxy.



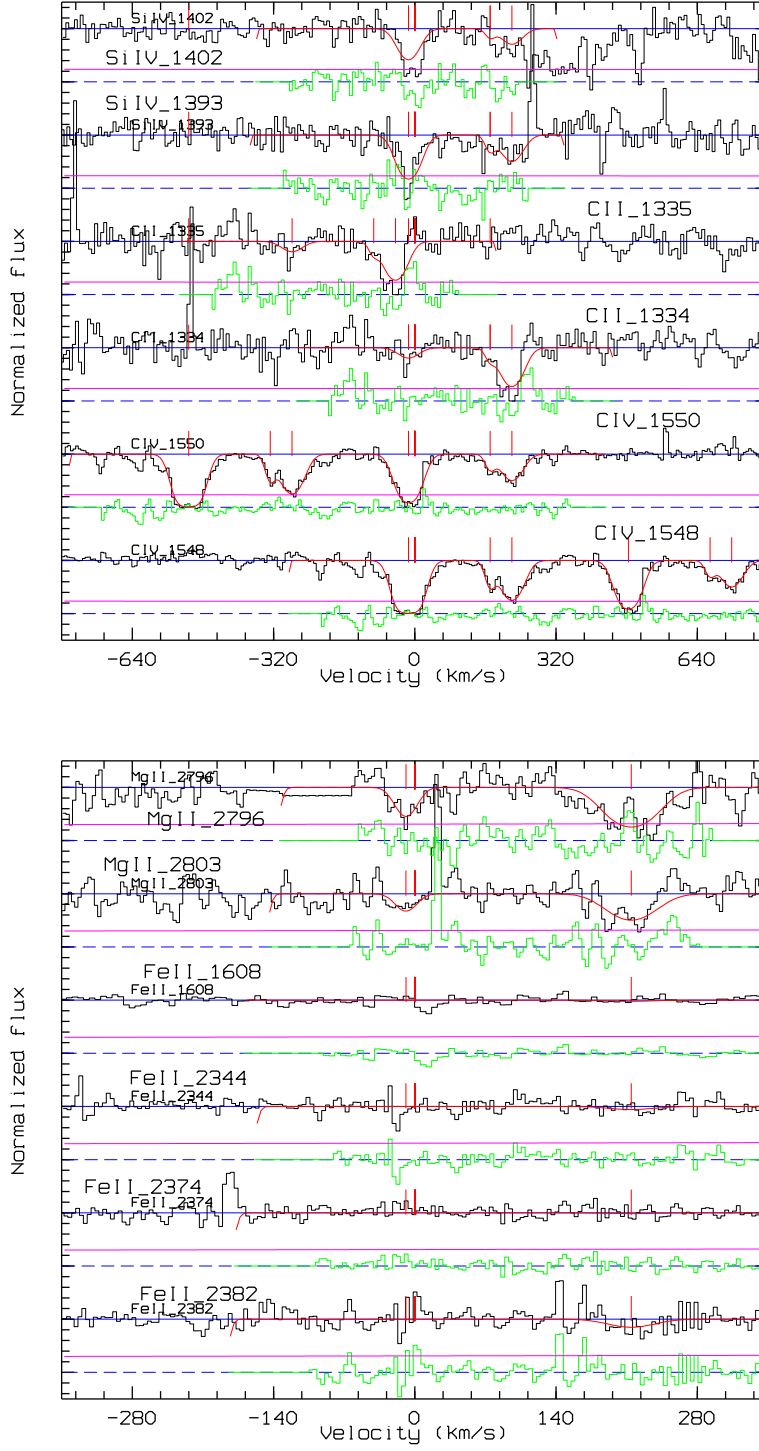


Fig. 5.— GRB 021004. Upper panel: UVES spectrum near the C IV  $\lambda\lambda$  1550, 1548, C II  $\lambda$ 1334, C II\*  $\lambda$ 1335, Si IV  $\lambda\lambda$ 1404, 1393 lines for the  $z=2.298$  and  $z=2.296$  systems in velocity space, along with the best fit model (solid line) and residuals (grey). Lower panel: same for the Fe II  $\lambda$ 2382, Fe II  $\lambda$ 2374, Fe II  $\lambda$ 2344, Fe II  $\lambda$ 1608, Mg II  $\lambda$ 2803 and Mg II  $\lambda$ 2796 lines. The zero in the velocity scale refers to  $z=2.296$ .

The detection of both high and low ionization lines, feasible thanks to the extremely wide spectral coverage achieved by UVES, allows us to obtain constraints on the ionization status of the gas responsible for the UV absorption, by comparing ion column density ratios with the predictions of photoionization codes. Unfortunately we were not able to measure column densities of different ions of the same element, except for C II/C IV and Al II/Al III for system z=2.328\_A, and C II/C IV for system z=2.298. In the other cases we are forced to use ratios of column densities of different ions of different elements in this analysis. These estimates of the gas ionization parameter are therefore somewhat degenerate with respect to relative element abundances. We used the Grevesse & Anders (1989) meteoritic abundances with extensions by Grevesse et al. (1993).

Figure 6 shows the logarithmic ratio between the C IV, C II, Fe II, Al II and Mg II column densities and that of Si IV for the six absorption systems as a function of the velocity shift with respect to the redshift of the host galaxy. No large variation of the ion ratios are seen for the six systems. We compared these line ratios to the predictions obtained by simulating a gas cloud illuminated by an ionizing continuum. We used Cloudy (vs 90.04, Ferland et al. 2002) to build grids of photoionization models as a function of U, the ionization parameter. U is defined as the ratio between the ionizing photon density and the electron density of the gas. It is computed assuming a constant density profile throughout the cloud, and a plane parallel geometry. We studied gas densities between  $1 \text{ cm}^{-3}$  and  $10^8 \text{ cm}^{-3}$ . The ionizing continuum was assumed to be a power law,  $F(E) = E^{-\Gamma}$  photons  $\text{cm}^{-2} \text{ s}^{-1}$ , with cutoffs at low and high energies. The high energy cutoff is fixed at  $10^{21} \text{ Hz}$ , while we run the simulations for different low energy cutoffs, from  $10^{10} \text{ Hz}$  to  $10^{14} \text{ Hz}$ . We produced several sets of simulations with  $\Gamma$  in the range 1–2. The ionizing continuum is constant in time. GRBs are highly variable sources and the ionization structure of the gas can be better studied using a time-dependent photoionization code, such as those of Nicastro et al. (1999) and Perna & Lazzati (2002). Nevertheless, our simpler approach is

Table 5: **GRB 021004. Logarithmic ion column densities in  $\text{cm}^{-2}$**

System	v. shift <sup>a</sup>	Si IV	C IV	C II	C II*	Al II	Fe II	Mg II
2.328_A	0	15.30±0.56	>15.2	13.40±0.45	13.90±0.58	13.55±0.35 <sup>c</sup>	13.34±0.15	13.82±0.24
2.328_B	−139	14.27±0.16	>14.4	<13.2	<13.2	12.23±0.35	12.53±0.24	12.93±0.60
2.328_C	−224	13.24±0.17	14.40±0.11	<13.2	<13.2	<12.0	<12.3	<12.8
2.321	−632	14.11±0.08	15.04±0.05	<13.2	<13.2	<12.0	<12.3	<12.8
2.298	−2729	13.43±0.33	14.16±0.20	14.28±0.20 <sup>b</sup>	<13.2	<12.0	12.68±0.20	13.22±0.10
2.296	−2913	13.79±0.16	14.72±0.25	13.43±0.40	<sup>b</sup>	<12.0	<12.3	12.68±0.21

errors, upper and lower limits are 90% confidence intervals; <sup>a</sup>km/s; <sup>b</sup> the z=2.296 C II\* line is completely blended with the z=2.298 C II line; <sup>c</sup> for system z=2.328\_A we measured also a column density of Al III of 13.66±0.30.

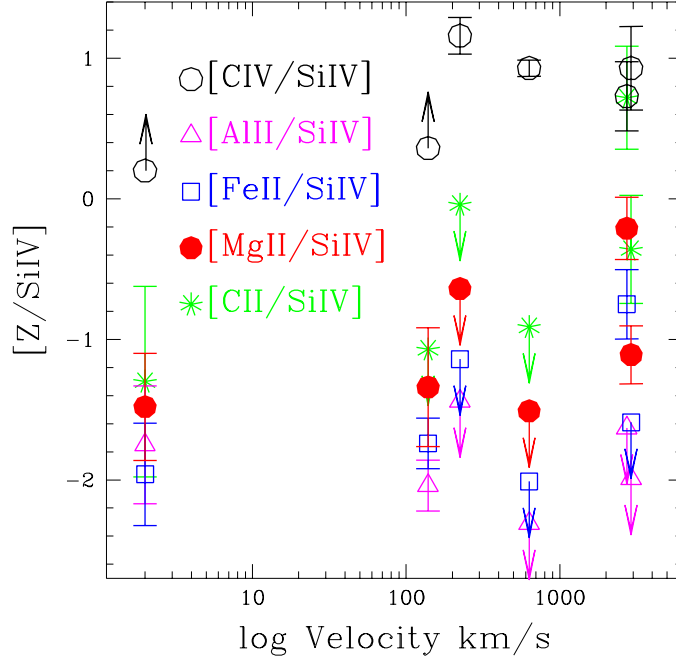


Fig. 6.— The logarithmic ratio between the C IV, C II, Fe II, Al II and Mg II column densities to that of Si IV for the six absorption systems as a function of the negative velocity shift with respect to the redshift of the host galaxy.

instructive in identifying general trends.

The predicted photoionization equilibrium ion ratios of  $[\text{Mg II}/\text{Si IV}]$ ,  $[\text{Fe II}/\text{Si IV}]$ ,  $[\text{Al II}/\text{Si IV}]$  and  $[\text{C IV}/\text{Si IV}]$  are shown in figure 7 for  $\Gamma = 2$  and  $n=1 \text{ cm}^{-3}$  and figure 8 for  $\Gamma = 2$  and  $n=10^8 \text{ cm}^{-3}$ . For each of the six redshift systems, thick segments superimposed on these curves indicate our 90% confidence determinations for these ratios. In figure 7 (for  $n=1 \text{ cm}^{-3}$ ) the  $[\text{Mg II}/\text{Si IV}]$ ,  $[\text{Fe II}/\text{Si IV}]$  and  $[\text{Al II}/\text{Si IV}]$  ion ratios for the systems  $z=2.328\_A$ ,  $z=2.328\_B$ ,  $z=2.328\_C$ , and  $z=2.296$  are all consistent with the same ionization status. For the system  $z=2.328\_A$  we measured the column density of Al II and Al III. Also their ratio is consistent with the ionization parameter inferred from the above ion ratios, see figures 7 and 8. For the same system we measured the column density of C II. The  $[\text{C II}/\text{Si IV}]$  ion ratio indicates a ionization parameter somewhat higher than that indicated by the other ion ratios for  $n=1 \text{ cm}^{-3}$  (see figure 7), while for  $n=10^8 \text{ cm}^{-3}$  the ionization parameter is fully consistent with that indicated by the other ion ratios (figure 8). The system at  $z=2.298$  shows a ionization parameter lower than that of system  $z=2.328\_A$ , while the system at  $z=2.321$  shows a higher ionization parameter. However, all ionization

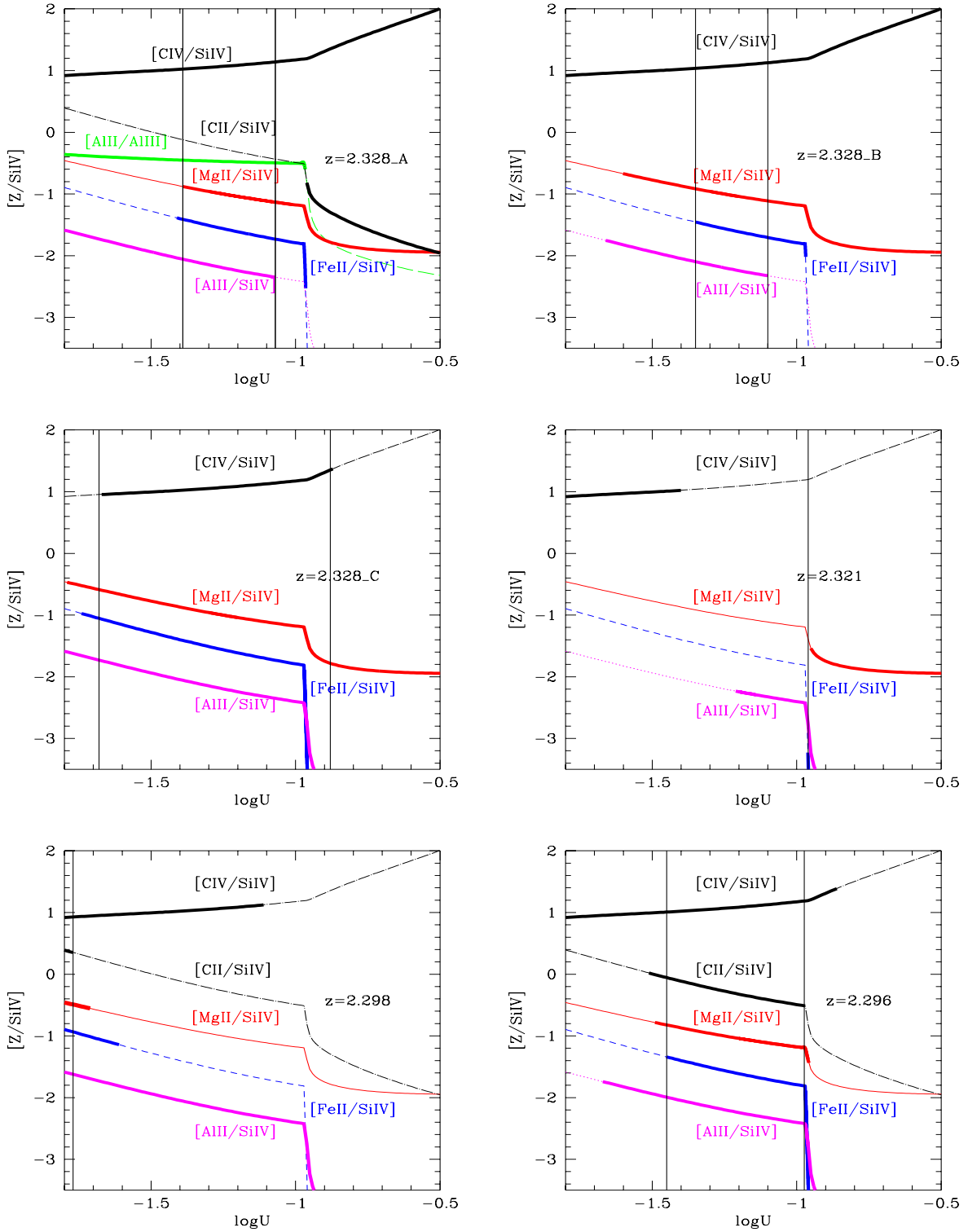


Fig. 7.— Ion ratios from CLOUDY models for the six absorption systems, assuming a gas density of  $1 \text{ cm}^{-3}$ :  $[\text{Mg II}/\text{Si IV}]$  = solid red curves,  $[\text{Fe II}/\text{Si IV}]$ = dashed blue curves,  $[\text{Al II}/\text{Si IV}]$  = dotted magenta curves and  $[\text{C IV}/\text{Si IV}]$  and  $[\text{C II}/\text{Si IV}]$ = dot-dashed black curves. The line indicating the model values is thick when it is consistent within 90% with the measured ion ratios. The vertical solid lines mark the range of allowed  $U$  values in each panel.

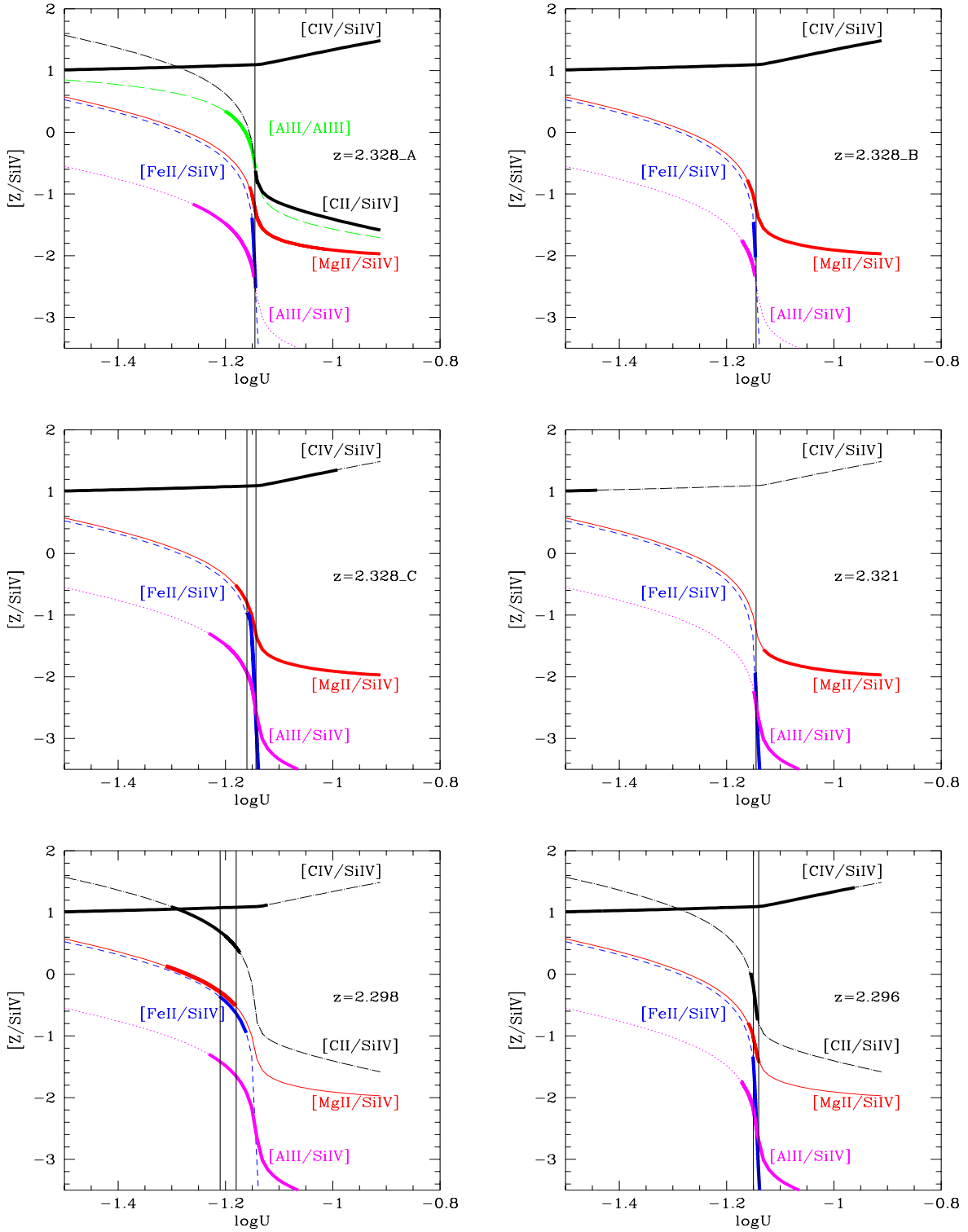


Fig. 8.— Ion ratios from CLOUDY photoionization models for the six absorption systems assuming a gas density of  $10^8 \text{ cm}^{-3}$ . Curves as in figure 7. The line indicating the model values is thick when it is consistent within 90% with the measured ion ratios, as in figure 7. The vertical solid lines mark the allowed  $U$  values in each panel.

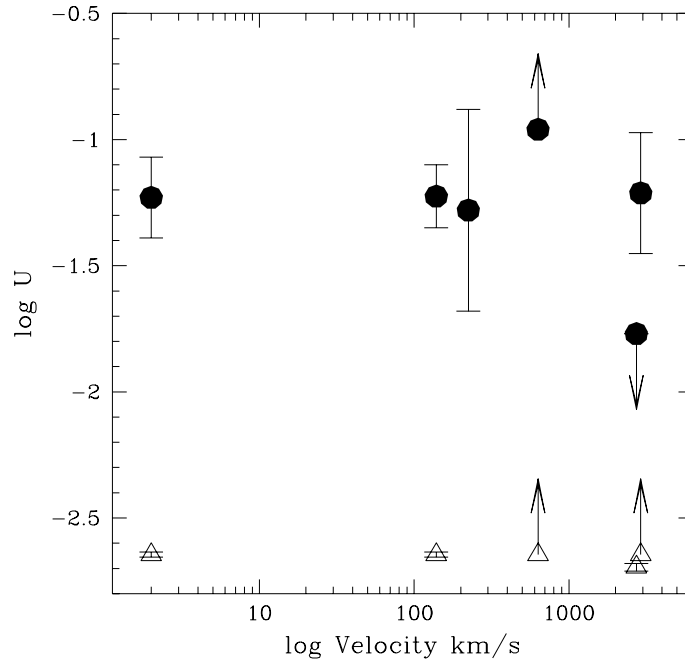


Fig. 9.— The logarithm of the best fit ionization parameters from figure 7 ( $n=1 \text{ cm}^{-3}$  filled circles) and from figure 8 ( $n=10^8 \text{ cm}^{-3}$ , open triangles, shifted by  $\log U=-1.5$ ), as a function of the velocity shift with respect to the redshift of the host galaxy. Error-bars and upper limits represent the purely statistical 90% confidence intervals.

parameters systems are consistent with a remarkably narrow range:  $10^{-1.7} < U < 10^{-1}$ , for  $n=1 \text{ cm}^{-3}$  and  $10^{-1.2} < U < 10^{-1}$ , for  $n=10^8 \text{ cm}^{-3}$  see figure 9, which plots the ionization parameters as a function of the velocity for the six systems. We note that in these ranges of  $U$  the  $[\text{Fe II}/\text{Mg II}]$  ratio varies by less than 30%, and the value found for the three systems in which we detect Fe II and Mg II lines ( $[\text{Mg II}/\text{Fe II}] \approx 0.4$ ) is consistent with what is expected from meteoritic abundances (and as was adopted for the CLOUDY calculations). This value is also in the range found for the Galactic ISM  $0.1 < [\text{Mg}/\text{Fe}] < 0.8$ . It is somewhat higher than that found by Savaglio et al. (2004) in a sample of faint K-band selected galaxies at  $1.4 < z < 2.0$   $-0.84 < [\text{Mg}/\text{Fe}] < 0.13$ . Assuming meteoritic abundances the hydrogen column density of the densest system ( $z=2.328_{\text{A}}$ ) is  $\gtrsim 5 \times 10^{19} \text{ cm}^{-2}$ , where the equality yields if all Si is in the form of Si IV. This column is so low that would have easily escaped detection in the Chandra X-ray spectrum (Butler et al. 2003) and it is consistent with the upper limit given by Moller et al. (2003).

Qualitatively similar results are drawn from the analysis of the  $n=10^8 \text{ cm}^{-3}$  curves, although the range of acceptable ionization parameters for the 6 systems is narrower, see figure 8. Qualitatively similar results were also obtained for the  $\Gamma = 1$  models.

### 3.1.1. The $z=2.328_{\text{A}}$ system

For this system we detect the C II\* $\lambda$ 1335 fine structure line. Unfortunately, the C II $\lambda$ 1334 ground state line is barely visible (with a signal to noise of just 2). The presence of a strong C II\* line suggests either a high gas density or a strong radiation field (Srianand & Petitjean 2000, 2001, Silva & Viegas 2002). C II\* and Si II\* fine structure lines have been detected in two other GRBs: GRB 020813 (Savaglio & Fall 2004) and GRB 030323 (Vreeswijk et al. 2004). Their ratio can be used to constrain the gas density or the radiation field (if both lines are detected one may solve for both variables, as shown by Srianand & Petitjean 2000), so their detection in GRB spectra looks very promising to constrain the physical properties of the absorbing gas.

For this system the C IV line is strongly saturated and so it cannot be used together with the C II to constrain the gas ionization status. As discussed in the previous section, within rather large uncertainties, the  $[\text{C II}/\text{Si II}]$  would suggest for  $n=1 \text{ cm}^{-3}$  a ionization parameter somewhat higher than that indicated by all other line ratios, assuming meteoritic abundances. This may be explained by a slight under-abundance of C with respect to Si in this system. A similar conclusion applies to system  $z=2.321$ , see below.

The C IV $\lambda$ 1548 lines of the  $z=2.328_{\text{A,B}}$  and C systems are blended with the C IV $\lambda$ 1550

of the  $z=2.321$  system, suggesting the presence of line locking, as first reported by Savaglio et al. (2002). Line locking is usually interpreted as the signature of line radiation pressure acceleration (see e.g. Foltz et al. 1987, Srianand & Petitjean 2000).

### 3.1.2. The $z=2.321$ system

For this system (as for  $z=2.328_{\text{C}}$ ) we were able to detect C IV and Si IV absorption lines only. The upper limits on the Mg II and Fe II transition allow us to put a significant lower limit on the ionization parameter of  $U \gtrsim 10^{-1}$  for this system for a gas density of  $1 \text{ cm}^{-3}$  and  $U \gtrsim 10^{-1.2}$  for a gas density of  $10^8 \text{ cm}^{-3}$ . For  $n=1$ , this is higher than the values for the other systems at a confidence level better than 90%. The [C IV/Si IV] ratio is formally inconsistent with this higher ionization parameter, but the disagreement is marginal, taking into account that the C IV/Si IV curves in figures 7 and 8 are very flat, and therefore small differences in the observed C IV/Si IV ratio would translate in large differences in the ionization parameter. Also in this case the disagreement may be explained by a slight under-abundance of C with respect to Si.

### 3.1.3. The $z=2.296$ and $z=2.298$ systems

Given the relatively high velocity shift of about 3000 km/s between the  $z=2.296$  and  $z=2.298$  systems and the host galaxy redshift, there is the possibility, at least in principle, that these systems are not associated with the GRB host galaxy but rather are intervening systems. We evaluated the probability of finding intervening C IV systems within 3000 km/s from the GRB host galaxy, from the density distribution of C IV systems given in D’Odorico et al. (1998) and Petitjean & Bergeron (1994). The probability of finding by chance two systems with column densities equal or larger than those given in Table 5 for these two lowest redshift systems is  $1.2 \times 10^{-5}$ , while the probability for only one of these systems is 0.1% for the  $z=2.296$  system and 0.5% for the  $z=2.298$  system.

The  $z=2.298$  system has a ionization parameter  $< 10^{-1.7}$  at the 90% confidence level for a gas density of  $1 \text{ cm}^{-3}$  (around  $10^{-1.2}$  for a gas density of  $10^8 \text{ cm}^{-3}$ ). This is the lowest of the ionization parameters found in the 6 systems. Furthermore, for this system we detect a rather strong C II  $\lambda 1334$  ground state line but not the C II\*  $\lambda 1335$  high excitation line, see figure 5, again indicating a lower radiation field (or a lower gas density).

The observed wavelength of the  $z=2.298$  system C II  $\lambda 1334$  line coincides with the wavelength of the  $z=2.296$  C II\*  $\lambda 1335$  line (see Table 3). This may be a further indication



of line locking.

### 3.1.4. Intervening systems

Two main intervening systems are present along the line of sight to GRB 021004, one around  $z=1.60$  and the other around  $z=1.38$  (see eg. Mirabal et al. 2003, Moller et al 2003). The UVES high resolution spectrum of GRB 021004 allows an accurate study of these systems, which are split in several components (see Table 3).

The system at  $z=1.38$  consists at least 3 components at  $z=1.3807$  ( $z=1.38\_A$ ),  $z=1.3802$  ( $z=1.38\_B$ ),  $z=1.3795$  ( $z=1.38\_C$ ). The latter system is also split in several parts in the range 1.3793-1.3798. The total velocity range spanned by the system is  $\sim 180$  km/s. We detected the following lines belonging to this system: Si II $\lambda$ 1808, Al III $\lambda$ 1854, Fe II $\lambda$ 2344, Fe II $\lambda$ 2374, Fe II $\lambda$ 2586, Mg II $\lambda$ 2796,2803, and Mg I $\lambda$ 2852.

The system at  $z=1.60$  is made by at least 4 components at  $z=1.6028$  ( $z=1.60\_A$ ),  $z=1.6024$  ( $z=1.60\_B$ ),  $z=1.6019$  ( $z=1.60\_C$ ) and  $z=1.6014$  ( $z=1.60\_D$ ). The total velocity range spanned by the system is of  $\sim 160$  km/s. For this system we detected the following lines: Al II $\lambda$ 1670, Fe II $\lambda$ 2344, Fe II $\lambda$ 2374, Fe II $\lambda$ 2382, Fe II $\lambda$ 2586, Mn II $\lambda$ 2594, Fe II $\lambda$ 2600, Mn II $\lambda$ 2606, Mg II $\lambda$ 2796,2803, and Mg I $\lambda$ 2852.

We estimated the column densities of the ions of the intervening systems using the same fitting procedure used for the six systems associated with the GRB host galaxy. They are given in Table 6

Table 6: **Log. ion column densities in  $\text{cm}^{-2}$  of the GRB 021004 intervening systems**

System	v. shift <sup>a</sup>	Fe II	Mg II	Si II	Al III
$z=1.38\_A$	0	15.68 $\pm$ 0.16	13.23 $\pm$ 0.07	15.12 $\pm$ 0.20	13.02 $\pm$ 0.20
$z=1.38\_B$	-63	–	12.92 $\pm$ 0.32	–	–
$z=1.38\_C$	-150	14.75 $\pm$ 0.40	15.20 $\pm$ 0.70	–	–
System	v. shift <sup>a</sup>	Fe II	Mg I	Mg II	Al II
$z=1.60\_A$	0	13.69 $\pm$ 0.16	11.33 $\pm$ 0.26	13.54 $\pm$ 0.21	12.66 $\pm$ 0.27
$z=1.60\_B$	-46	12.63 $\pm$ 0.16	11.64 $\pm$ 0.18	12.95 $\pm$ 0.10	–
$z=1.60\_C$	-104	14.35 $\pm$ 0.18	12.80 $\pm$ 0.27	15.45 $\pm$ 0.80	13.24 $\pm$ 0.50
$z=1.60\_D$	-160	13.57 $\pm$ 0.10	11.82 $\pm$ 0.14	13.47 $\pm$ 0.06	12.58 $\pm$ 0.25

errors, upper and lower limits are 90% confidence intervals; <sup>a</sup>km/s

### 3.2. GRB 020813

For this GRB we considered the absorption systems at the following velocities with respect to the redshift of the host galaxy, which was assumed to be 1.255 (Barth et al. 2003):  $v=0$  km/s (system A in figure 10),  $v=-106$  km/s (system B) and  $v=-306$  km/s (system C). Note that the system A and system B lines are strongly blended with the exception of the Fe II2374 line. We also consider the system at  $z=1.2234$ .

We fitted simultaneously the 6 lines of the 3 absorption systems in figure 10. Table 7 gives for the 3 systems the best fit Fe II and Mg II abundances along with the velocity shift of each system with respect to the redshift of the host galaxy. Mg II lines of systems A and B are strongly saturated and therefore their column density estimates are more uncertain. Unfortunately the UVES spectrum covers a wavelength range much smaller than the Keck LRIS spectrum and several of the lines studied by Barth et al. (2003) and Savaglio & Fall (2004), in particular Zn II, Cr II, Si II, are not accessible.

We performed similar fits to the 5 lines associated with the  $z=1.2234$  system, split in two components. The results are in figure 11 and in Table 7.

Unfortunately in this case the redshift of the GRB is not high enough to have strong high ionization lines in the spectrum, and therefore we do not have a direct way to constrain the ionization status of the gas responsible for the UV absorption.

The [Fe II/Mg II] ratio is consistent with a constant value in the four systems. This ratio is also consistent with meteoritic abundances, assuming that the ionization parameter is in the range  $10^{-2.5} - 10^{-1}$ .

### 3.3. The $z=1.2234$ system

The system at  $z=1.2234$  is shifted by about 4200 km/s from the redshift of the host galaxy. The probability to find an Mg II intervening system with  $W_{\lambda 2796.35} = 1.3 \pm 0.03 \text{ \AA}$

Table 7: **GRB 020813, Logarithmic ion column densities in  $\text{cm}^{-2}$**

System	velocity shift <sup>a</sup>	Fe II	Mg II
$z=1.255\_A$	0.	$15.20 \pm 0.29$	$> 16.0$
$z=1.255\_B$	-106	$15.47 \pm 0.27$	$> 15.5$
$z=1.255\_C$	-306	$13.58 \pm 0.10$	$13.79 \pm 0.21$
$z=1.2234$	-4204	$13.96 \pm 0.18$	$> 16.0$

<sup>a</sup>km/s

(see Table 7) within this velocity range is  $\lesssim 1\%$ , using the distribution of Mg II systems given by Steidel & Sargent (1992). Although not as conclusive as in the case of the  $z=2.296$  and  $z=2.298$  systems in the spectrum of GRB 021004, we remark that this probability is rather small, and that the velocity shift with respect to the redshift of the host galaxy is intriguingly similar to that of the GRB 021004 systems.

#### 4. Discussion

GRB 021004 shows absorption systems which span  $\sim 3000$  km/s in velocity towards the observer (no receding system is detected). The systems are most likely local to the GRB since the probability of finding two or more different absorption systems along the line of sight by random fluctuations is negligible.

It has been suggested that radiative acceleration by the prompt GRB emission may be responsible for the high detected speeds (Schaefer et al. 2003). However, this seems unlikely since low ionization ions such Fe II and Mg II are present in the high velocity absorber. The radiative acceleration is dominated by the GRB and early afterglow radiation. It is therefore unlikely that recombination can be so rapid to have any influence on the acceleration of the absorbing material. In the photoionization phase each nucleon receives an amount of energy comparable to the ionization potential of the  $K$ -shell electron. For a solar metallicity plasma the acceleration is regulated by H atoms and, at the end of the photoionization, the absorbing material has an outward velocity of:

$$v_{\text{ion}} \sim \sqrt{\frac{h\nu_{\text{ion}}}{m_p}} \sim 50 \text{ km/s} \quad (1)$$

Once the gas is fully ionized, acceleration proceeds due to radiation pressure on free electrons through Inverse Compton (IC) interactions. For a burst of isotropic equivalent energy  $E_{\text{iso}}$  the IC acceleration is obtained by momentum conservation:

$$v_{\text{IC}} = \frac{E_{\text{iso}} \sigma_T}{4\pi R^2 m_p c} \sim 0.6 R_{18}^{-2} \text{ km/s} \quad (2)$$

we conclude that at the minimum distance of the absorbing medium  $R \sim 10^{18}$  cm (Lazzati et al. 2002; Heyl & Perna 2003; in order to be ahead of the fireball at the time at which absorption is detected) radiative acceleration is unable to propel the absorber to an outflowing speed comparable to the value(s) observed.

Possible explanations for the large outflowing speed are either a supernova exploded several years prior to the GRB (Vietri & Stella 1998) or a high velocity wind from the

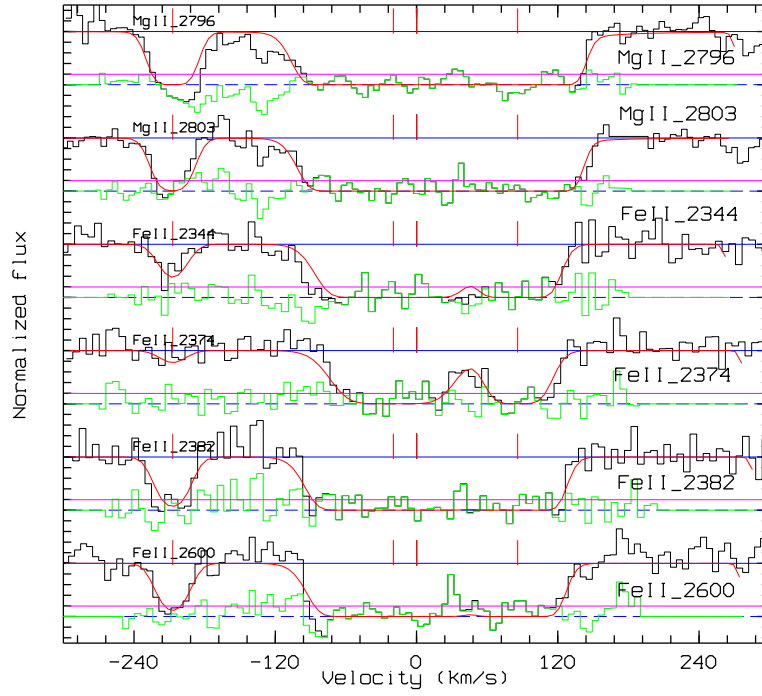


Fig. 10.— UVES spectrum of GRB 020813 near the Fe II  $\lambda$ 2600, Fe II  $\lambda$ 2382, Fe II  $\lambda$ 2374, Fe II  $\lambda$ 2344, Mg II  $\lambda$ 2803 and Mg II  $\lambda$ 2796 lines for the three absorption systems, in velocity space, along with the best fit model, solid line and residuals. The zero of the velocity scale refers to  $z=1.2545$

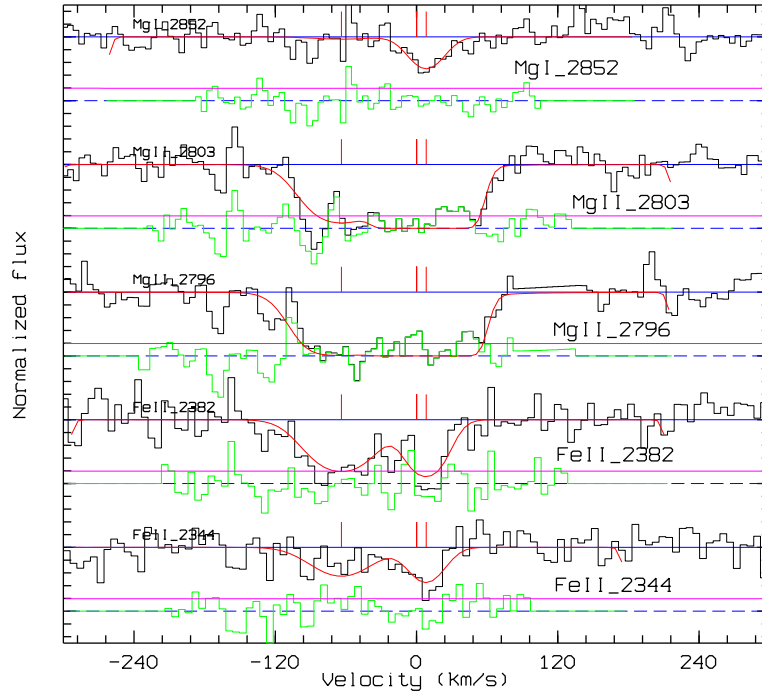


Fig. 11.— UVES spectrum of GRB 020813 near the Fe II $\lambda$ 2382, Fe II $\lambda$ 2344, Mg II $\lambda$ 2803, Mg II $\lambda$ 2796 and Mg I $\lambda$ 2852 lines for the  $z=1.2234$  absorption systems, in velocity space, along with the best fit model, solid line and residuals. The zero of the velocity scale refers to  $z=1.2234$

progenitor Wolf–Rayet (WR) star (MacFadyen & Woosley 1999; Schaefer et al. 2003; Mirabal et al. 2003). The large velocity spread with similar ionization parameter is however difficult to account for in a SNR scenario, where values around a typical expansion velocity would be expected. On the other hand, WR winds are known to be clumpy and velocities up to  $\sim 4000$  km/s were detected from P–Cygni profiles (Niedzleski & Skórzyński 2002).

In this work we derived physical parameters of the absorbers under the assumption of equilibrium conditions which,  $\sim 0.5$  days after the GRB explosion, are attained only if the electron density in the absorber is  $n \sim 10^{7-8} \text{ cm}^{-3}$ . Assuming equilibrium conditions, the total column density of the absorber can be computed from the ion column density corrected for the ionization fraction. Consider the Si IV line in the A system. The density is given by:

$$n = \frac{N_{\text{Si}}}{A_{\text{Si}} R \eta} \sim \frac{10^{15.3}}{4 \times 10^{-5} 10^{18} R_{18} 10^{-6} \eta_{-6}} \approx 5 \times 10^7 R_{18}^{-1} \eta_{-6}^{-1} \text{ cm}^{-3} \quad (3)$$

where  $R$  is the fireball radius at the time the lines were observed,  $A_{\text{Si}}$  is the Si abundance and  $\eta$  is the ratio of the width of the absorbing shell over its radius. The ionization parameters derived above and implications discussed here are therefore relevant only in the case of an extremely clumpy wind or SNR.

The photoionization results of CLOUDY yield an ionization parameter constrained in a relatively small range  $10^{-1.7} < U < 10^{-1}$ . In a single explosion GRB model, the ionization parameter scales with the square of the outflow velocity, since the absorber’s distance scales with velocity as well. Even though the ionization parameter depends on the electron density, it seems unlikely that density variations are such as to compensate for the large velocity difference. In a wind environment, on the other hand, the ionization parameter is constant since the photon density and particle density scale with the same power of the distance. The relatively small variations in the inferred  $U$ , which do not show any clear trend with velocity, can therefore be interpreted as density fluctuations on top of a regular  $R^{-2}$  wind density profile (as already discussed by e.g. Schaefer et al. 2003 and Mirabal et al. 2003).

Finally, we note that the Fe II and Mg II column densities found in GRB 020813 are 10–100 times higher than those in GRB 021004. This is likely due to a much higher ionization of the gas in the latter case, rather than a large difference in the total absorbing column of gas or to highly non solar metal abundances (note that in both cases the [Fe II/Mg II] ratio is consistent with meteoritic abundances). We also note the similarity between the velocity shift between the  $z=1.2234$  system and the GRB 020813 host galaxy and the shift of the  $z=2.296$  and  $z=2.298$  systems with respect to the GRB 021004 host galaxy. Although the probability for a chance occurrence of the  $z=1.2234$  system is not

as low as in the cases of the two shifted systems in GRB 021004, and that the  $z=1.2234$  ionization status is probably much lower than that of the  $z=2.296$  and  $z=2.298$  systems, this similarity might suggest a common scenario for the two GRBs.

## 5. Conclusions

One of the straightforward results of our UVES high resolution observations of two GRB afterglows is that the ISM of the host galaxies is complex, and many components contribute to each main absorption systems. These components span a total velocity range of up to about 3000 km/s. Several narrow components are resolved down to a width of a few tens of km/s. The UVES wide band coverage allowed us to investigate simultaneously both high ionization lines such as C IV and Si IV, and low ionization lines such as Mg II and Fe II in GRB 021004. This allowed us to constrain the ionization parameter of the gas of the different absorption systems. Combined with photoionization results obtained with CLOUDY the ionization parameters appear to lie in a relatively small range, with no clear trend with the system velocity. This can be interpreted as density fluctuations on top of a regular  $R^{-2}$  wind density profile. The [Mg II/Fe II] ratio of  $\approx 0.4$  found for systems  $z=2.328\_A$ ,  $z=2.328\_B$ , and  $z=2.298$  is consistent with what is expected from meteoritic abundances. Assuming these abundances, the measured Si IV column density for system  $z=2.328\_A$  implies a lower limit of  $\gtrsim 5 \times 10^{19} \text{ cm}^{-2}$  to the system total hydrogen column density.

Indeed, our study shows that rapid reaction to the GRB triggers, high resolution and wide spectral coverage are the key ingredients to study GRB host galaxies. Today observations of this kind are still difficult and rather episodic. However, they should become routine after the launch of the *Swift* satellite, also thanks to the development of a dedicated Rapid Response observing Mode for the VLT telescopes. This mode will make possible automatic follow-up of GRBs (or other transient events) with response times in the 10m–1hr range, therefore helping in gathering spectra of unprecedented quality of medium to high redshift GRB host galaxies.

We acknowledge support from contract ASI/I/R/390/02 and MIUR grant Cofin–2003–41. We thank Fabrizio Nicastro and Emanuele Giallongo for useful discussions, Sandra Savaglio for her early work on this program, and an anonymous referee for comments that helped to improve the presentation.

## REFERENCES

- Akerlof, C., Balsano, R., Barthelemy, S. et al. 1999, *Nature*, 398, 400
- Barth, A.J., Sari, R., Cohen, M.H. 2003, *ApJ*, 584, L47
- Butler, N.R., Marshall, H.L, Ricker, G.R. et al. 2003, *ApJ*, 597, 1010
- Covino, S., Malesani, D. Tavecchio, F. et al. 2003, *A&A*, 404, L5
- Dekker, H., D’Odorico, S., Kaufer, A., Delabre, B., & Kotzlowski, H. 2000, *The International Society for Optical Engineering*, 4008, 534
- Della Valle, M. Malesani, D., Benetti, S. et al. 2003, *A&A*, 406, L33
- D’Odorico, V., Cristiani, S., D’Odorico, S., Fontana, A., Giallongo, E. 1998, *A&AS*, 127, 217
- Ferland, G.S. 2002, University of Kentucky Dept. of Physics and Astronomy, Internal Report
- Fiore, F. et al. 2002, *GCN* 1524
- Foltz, C.B., Weymann, R.J., Morris, S.L., Turnshek, D.A. 1987, *ApJ*, 317, 450
- Fontana, A. & Ballester, P. 1995, *The ESO Messenger*, 80, 37
- Fox, D.W., Blake, C., Price, P.A. 2002, *GCN Circ.* 1470
- Fox, D.W. 2002, *GCN Circ.* 1564
- Fox, D.W., Yost, S, Kulkarni, S.R. et al. 2003, *Nature*, 422, 284
- Galama, T.J., Vreeswijk, P. M., van Paradijs, J. et al. 1998, *Nature*, 395, 670
- Galama, T.J., Briggs, M.S., Wijers, R.A.M. et al. 1999, *Nature*, 398, 394
- Gladders, M. & Hall, P. 2002, *GCN Circ.* 1472
- Grevesse, N. & Anders, E. 1989, *AIP Conference Proceedings*, Vol. 183. New York, American Institute of Physics, p. 1-8.
- Grevesse, N., Noel, A. & Sauval, A.J., 1993, *A&A*, 271, 587
- Heyl, J. S. & Perna, R. 2003, *ApJ*, 586, L13



- Hjorth, J., Sollerman, J., Moller, P. et al. 2003, *Nature*, 423, 847
- Holland, S.T., Weidinger, M., Fynbo, J.P.U. et al. 2003, *AJ*, 125, 2291
- Lazzati, D., Rossi, E., Covino, S., Ghisellini, G., & Malesani, D. 2002, *A&A*, 396, L5
- MacFadyen, A.I. & Woosley, S.E. 1999, *ApJ*, 524, 262
- Mirabal, N., Halpern, J. P., Chornock, R. et al. 2003, *ApJ*, 595, 935
- Matheson, T., Garnavich, P. M., Foltz, C., et al. 2003, *ApJL*, 582, L5
- Moller, P. et al. 2003, *A&A*, 396, L21
- Nicastro, F., Fiore, F., Perola, G.C., Elvis, M. 1999, *ApJ*, 512, 184
- Niedzlieski, A. & Skórzyński, W., 2002, *Acta Astronomica*, 52, 81
- Paczynski, B. 1998, *ApJL*, 494, L45
- Perna, R. & Lazzati, D. 2002, *ApJ*, 580, 261
- Petitjean, P. & Bergeron, J. 1994, *A&A* 283, 759
- Pettini, M., Smith, L.J., King, D.L., Hunstead, R.W. 1997, *ApJ*, 486, 665
- Price, P.A. et al. 2003, *Nature*, 423, 844
- Savaglio, S. et al. 2002, *GCN* 1633
- Savaglio, S., Fall, S.M., Fiore, F. 2003, *ApJ*, 585, 638
- Savaglio, S., Glazebrook, K., Crampton, D. et al. 2004, *ApJ*, 602, 51
- Savaglio, S., Fall, S.M. 2004, *ApJ*, 614, 293
- Silva, A.I., & Viegas, S.M. 2002, *MNRAS*, 329, 135
- Shirasaki, Y. et al. 2002 *GCN* 1565
- Srianand, R. & Petitjean, P. 2000, *A&A*, 357, 414
- Srianand, R. & Petitjean, P. 2001, *A&A*, 373, 816
- Stanek, K.Z., Matheson, T., Garnavich, P. M. et al. 2003, *ApJ*, 591L, 17
- Steidel, C.C. & Sargent, W.L.W. 1992, *ApJS*, 80, 1

- Steidel, C.C., Adelberger, K.L., Giavalisco, M., Dickinson, M., Pettini, M. 1999, ApJ, 519, 1
- Schaefer, B.E., Gerardy, C.L., Hflich, P. et al., 2003, ApJ, 588, 387
- Turnshek, D.A., Wolfe, A.M., Lanzetta, K.M. et al. 1989, ApJ, 344, 567
- Vietri, M. & Stella, L. 1998, ApJ, 507, L45
- Villasenor et al. 2002, GCN 1471
- Vreeswijk, P.M., Ellison S.L., Ledoux, C. et al. 2004, A&A, 419, 927
- Woosley, S. E. 1993, ApJ, 405, 273